Digital Communications and Networks 7 (2021) 55–61

Contents lists available at ScienceDirect

Digital Communications and Networks

journal homepage: www.keaipublishing.com/dcan

Joint MAP channel estimation and data detection for OFDM in presence of phase noise from free running and phase locked loop oscillator

Kamayani Shrivastav [a,*], R.P. Yadav [a], K.C. Jain [b]

[a] Department of Electronics and Communication, Malaviya National Institute of Technology, 302017, India
[b] Department of Mathematics, Indian Institute of Information Technology, Kota, India

ARTICLE INFO

Keywords:
Orthogonal frequency division multiplexing
Phase noise
Free running oscillator
Phase-locked loop oscillator
Maximum a posteriori
Channel estimation
Data detection

ABSTRACT

This paper addresses a computationally compact and statistically optimal joint Maximum a Posteriori (MAP) algorithm for channel estimation and data detection in the presence of Phase Noise (PHN) in iterative Orthogonal Frequency Division Multiplexing (OFDM) receivers used for high speed and high spectral efficient wireless communication systems. The MAP cost function for joint estimation and detection is derived and optimized further with the proposed cyclic gradient descent optimization algorithm. The proposed joint estimation and detection algorithm relaxes the restriction of small PHN assumptions and utilizes the prior statistical knowledge of PHN spectral components to produce a statistically optimal solution. The frequency-domain estimation of Channel Transfer Function (CTF) in frequency selective fading makes the method simpler, compared with the estimation of Channel Impulse Response (CIR) in the time domain. Two different time-varying PHN models, produced by Free Running Oscillator (FRO) and Phase-Locked Loop (PLL) oscillator, are presented and compared for performance difference with proposed OFDM receiver. Simulation results for joint MAP channel estimation are compared with Cramer-Rao Lower Bound (CRLB), and the simulation results for joint MAP data detection are compared with "NO PHN" performance to demonstrate that the proposed joint MAP estimation and detection algorithm achieve near-optimum performance even under multipath channel fading.

1. Introduction

The conventional OFDM receivers, without attending the substantial effect of PHN in joint, severely degrade the Mean Square Error (MSE) performance for channel estimation and Symbol Error Rate (SER) performance for data detection [1–3]. Thus reliable channel estimation and data detection incorporate the functionality of PHN estimation in joint [4–11].

The Maximum Likelihood (ML) based joint channel estimator of [4] utilizes the approach of forward and backward substitution with small PHN approximation in the frequency domain. In Ref. [5], the Monte Carlo method based on Expectation Minimization (EM) for channel estimation is proposed. In EM channel estimation, the non-Gaussianity of posterior Probability Density Function (PDF) of hidden variables that are random parameters without direct observance is the main problem. This problem has been solved in Ref. [5] by point density estimation with high Computational Complexity (CC). In Ref. [6], Basis Expansion Model (BEM) coefficients are jointly estimated with very high CC, while the joint covariance matrix of phase and channel is already known. In Ref. [7], the two-stage time-domain MAP estimation of Common Phase Error (CPE) corrupted CIR is not fully joint in the channel estimation stage. With high CC, the frequency domain joint MAP approach of [8] obeys the deterministic restriction with the assumption of small PHN and uses a prior known statistics of PHN and data both. The blind compensation of PHN is proposed in Ref. [9], where time-averaged PHN is approximated over sub-blocks. This type of PHN realization may be corrupted in frequency selective fading. In Ref. [10], with joint ML approach, PHN Discrete Fourier Transform (DFT) coefficient matrix is approximated with one of the entries of codebook with an assumption of equal probability. The joint MAP technique of [11] is code-aided synchronization with the EM framework.

A new approach to derive the joint MAP cost function for the channel estimation/data detection and PHN estimation in the frequency domain is introduced in this paper. The proposed joint MAP estimator/detector utilizes the prior statistical knowledge of PHN spectral components without the restriction of small PHN. The statistical properties of PHN spectral components are also analysed for their impact on system performance. Further, a statistically optimal and computationally compact

* Corresponding author.
E-mail address: 2014rec9012@mnit.ac.in (K. Shrivastav).

https://doi.org/10.1016/j.dcan.2020.09.007
Received 16 April 2018; Received in revised form 2 September 2020; Accepted 22 September 2020
Available online 26 September 2020

solution of the joint estimation/detection is produced with the proposed cyclic gradient descent optimization algorithm to minimize the cost function.

This paper focuses on a more enhanced PHN model as the Ornstein-Uhlenbeck process [12], as well as the most studied model in Ref. [13] as the Wiener process. For the rest of the paper, in section 2, the modelling of PHN for both the oscillators, i.e., FRO and PLL oscillator, is presented, and after that, a PHN corrupted OFDM signal model in the frequency domain is derived in section 3. Section 4 discusses the joint MAP estimator and detector, which performs efficient channel estimation and data detection even with receiver PHN impairments. An iterative cyclic gradient descent optimization algorithm is proposed in section 5 to minimize the MAP cost function globally with respect to channel/data and PHN in joint. Section 6 manifests the competence of the proposed algorithm in regards to computational complexity. Simulation results are presented in section 7, and section 8 concludes the paper.

2. Phase noise modelling

The PHN is the random fluctuation in the phase of the sinusoidal waveform used for frequency up/down conversion of baseband signals to/from Radio Frequency (RF). If the time-varying PHN process, $(\theta(t))$, which is sampled with the sampling interval, T_s/N, means $\theta_n = \theta(nT_s/N)$ where $n = 0,\ 1,\ 2,\ \ldots,\ N-1$, then

$$\theta_{n+1} = \theta_n e^{-\phi\frac{T_s}{N}} + \mu\left(1 - e^{-\phi\frac{T_s}{N}}\right) + \varphi_n \tag{1}$$

where μ is asymptotic mean, ϕ is the drift and σ^2 is the variance of the noise present in the system which is white noise in our case. φ_n is a sequence of Identically and Independently Distributed (iid) random variables with mean zero and variance ${\sigma_{\varphi_n}}^2$. If we take no drift in the process, $\phi = 0,$ then equation (1) is:

$$\theta_{n+1} = \theta_n + \varphi_n \tag{2}$$

which is the Wiener process [13]. PHN from FR Voltage Controlled Oscillator (VCO) follows the Wiener process of equation (2) with PDF, $\Pr(\varphi_n) = \mathcal{N}(0, \sigma_\varphi^2)$, with zero mean and variance, $\sigma_\varphi^2 = {\sigma_{\varphi_n}}^2 = 2\pi\beta T_s/N$, where β, T_s and N are PHN 3-dB bandwidth, OFDM symbol duration and number of subcarriers, respectively.

Though PHN from the PLL VCO follows the regular O–U process [12], but for wide sense stationary output from the PLL [14], asymptotic mean should be zero, thus

$$\theta_{n+1} = \theta_n e^{-\phi\frac{T_s}{N}} + \varphi_{PLLn} \tag{3}$$

where φ_{PLLn} is a sequence of iid random variables with mean zero and variance (See Appendix):

$$\sigma^2_{\varphi_{PLLn}} = 4\pi^2 f_c^2\left(C_{in}\frac{T_s}{N} + 2\sum_{i=1}^{2}(\xi_i + \zeta_i)\left(1 - e^{-\lambda_i\frac{T_s}{N}}\right)\right). \tag{4}$$

If $\theta^m = [\theta^m_0, \theta^m_1, \ldots \theta^m_{N-1}]^T$ is the PHN vector for the m^{th} OFDM symbol then,

$$\mathrm{P}^m = \left[p^m_{-\frac{N}{2}}, p^m_{-\frac{N}{2}+1}, \ldots, p^m_0, \ldots, p^m_{\frac{N}{2}-2},\ p^m_{\frac{N}{2}-1}\right]^T \tag{5}$$

defines a vector of the DFT coefficients of one realization of $e^{j\theta_n}$ during m^{th} OFDM symbol where

$$p^m_k = \frac{1}{N}\sum_{n=0}^{N-1} e^{j\theta^m_n} e^{\frac{-j2\pi nk}{N}},\ -\frac{N}{2} \le k \le \frac{N}{2} - 1. \tag{6}$$

The correlation matrices for FR VCO and PLL VCO are respectively given as [2,15]:

$$\mathbf{R}_{\mathrm{P}^m}(a,b) = \frac{1}{N^2}\sum_{u=0}^{N-1}\sum_{v=0}^{N-1} e^{\frac{-|u-v|\sigma^2_\varphi}{2}} e^{\frac{-j2\pi(au-bv)}{N}},\quad -\frac{N}{2} \le a,\ b \le \frac{N}{2} - 1 \tag{7}$$

and

$$\mathbf{R}_{\mathrm{P}^m}(a,b)_{PLL} = \frac{1}{N^2}\sum_{u=0}^{N-1}\sum_{v=0}^{N-1} e^{-\frac{j2\pi(au-bv)}{N}} e^{-4\pi^2 f_c^2\left(C_{in}\frac{|u-v|\text{dntre frequency in Hz is } T_s}{N} + 2\sum_{i=1}^{2}(\xi_i+\zeta_i)\left(1 - e^{-\lambda_i\frac{|u-v|T_s}{N}}\right)\right)},\quad -\frac{N}{2} \le a,\ b \le \frac{N}{2} - 1 \tag{8}$$

As the cumulative PHN increment between two samples of the received signal is a Gaussian random variable and θ_n modelled as Wiener process and asymptotically Gaussian random variable for θ_n modelled as celebrated O–U process, P^m is complex Gaussian distributed, $\Pr(\mathrm{P}^m) = \mathcal{CN}(0, \mathbf{\Theta})$, with mean zero and covariance matrix, $\mathbf{\Theta} = \mathbf{R}_{\mathrm{P}^m}(a,b)$ for FR VCO and $\mathbf{\Theta} = \mathbf{R}_{\mathrm{P}^m}(a,b)_{PLL}$ for PLL VCO.

Since the Power Spectral Density (PSD) of PHN tappers off rapidly beyond the loop bandwidth, PHN process can be sufficiently characterized by a few lower order spectral components, containing most of the energy of a PHN sequence. These lower order spectral components of PHN are given by ${p_0}^m, {p_1}^m, {p_{-1}}^m, {p_2}^m, {p_{-2}}^m,$ etc. Here we define a variable Q as an approximation order for which $2Q+1$ elements of the vector P^m, *i.e.*, $p^m_{-Q}, \ldots, p^m_0, \ldots, p^m_Q$, can well approximate the PHN process.

Results for the matrix $\mathbf{\Theta}$ are evaluated and presented in Fig. 1 (a) and 1 (b) for FR VCO and PLL VCO, respectively, corresponding to IEEE 802.11g like a system with 64 subcarriers, 20 MHz baseband sampling frequency and 20 kHz PHN 3-dB bandwidth. Though the time-varying PHN process of FR VCO can be characterized with PHN 3-dB BW only, PLL VCO requires more parameters to characterize such as $f_c = 5GHz$, loop corner frequency is 20 kHz, $C_{in} = 10^{-25}s$ and $C_{VCO} = 10^{-19}s$. It is assumed that the VCO is more noisy than reference oscillator, $C_{PLL} = 4{*}10^8\ /s^2$. By comparing Fig. 1(a) and (b), it can be observed that PLL VCO tends to reduce the overall PHN as well as the near carrier PHN significantly. It can also be concluded from the Fig. 1 (a) and (b) that, although the cross correlation terms are significant for some lower order PHN spectral components only, the cross correlation of these PHN spectral components cannot be neglected when compared with auto correlation terms.

3. OFDM system modelling

In this work, we are considering packet transmission of OFDM symbols. A packet (Fig. 2) consists of several consecutive OFDM symbols with a few initial full pilot symbols followed by pay load in which data and pilot subcarriers are multiplexed together. At the receiver side, full pilot symbols are used for channel estimation while the data vector is assumed to be known, and when the payload is received, the channel is assumed to be exactly known.

Further, we model an OFDM system consisting of N subcarriers with the sampling instant T_s/N. If $X^m_k, k = 0, 1, \ldots, N-1,$ is the frequency domain Quadrature Amplitude Modulation (QAM) modulated symbol on k^{th} subcarrier of m^{th} symbol, then $\mathrm{X}^m = [X^m_0, X^m_1, \ldots, X^m_{N-1}]^T$ defines a

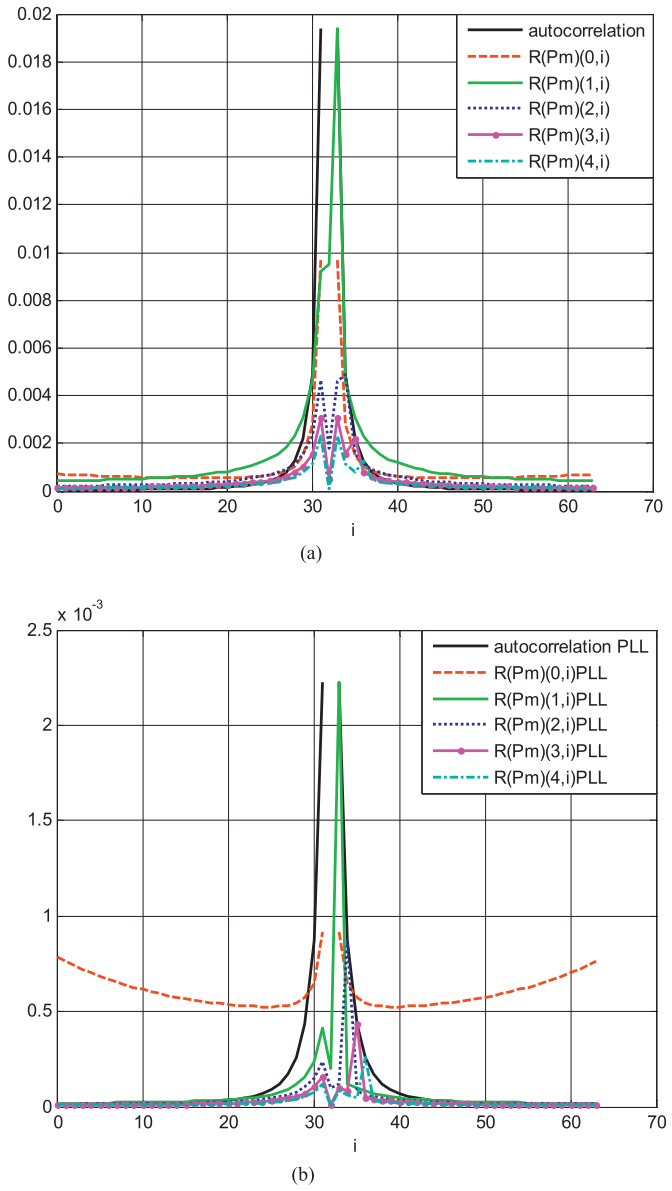

Fig. 1. Correlation property of PHN spectral components (a) FR VCO (b) PLL VCO.

symbol vector. Consequently, the n^{th} sample of the discrete time base-band signal after taking Inverse Fast Fourier Transform (IFFT) is

$$S_n^m = \frac{1}{N}\sum_{k=0}^{N-1} X_k^m e^{\frac{j2\pi kn}{N}}, \quad 0 \le n \le N-1. \tag{9}$$

Before transmitting over the channel, this signal is preceded with Cyclic Prefix (CP) of length N_{CP} samples and duration T_{cp} so that it is longer than the channel impulse response. This implies that there is no

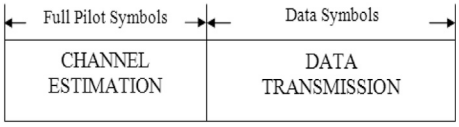

Fig. 2. OFDM packet structure.

Inter Symbol Interference (ISI) in the windows of N samples (the effect of multipath is still experienced within each symbol). After this, the signal is transformed back to the serial form and is up- converted to RF and finally is sent over the channel. If the discrete time composite CIR with order L is denoted by $g(l)$ and the CTF on the k^{th} subcarrier is denoted by h_k, then

$$h_k = \sum_{l=0}^{L-1} g(l) e^{\frac{-j2\pi kl}{N}}. \tag{10}$$

Denoting the discrete time receiver PHN process and Additive White Gaussian Noise (AWGN) impairment to the m^{th} symbol by θ_n^m and w_n^m, respectively, the received OFDM signal after conversion and CP removal can be written as

$$r_n^m = \left[S_n^m \otimes g(n)\right] e^{j\theta_n^m} + w_n^m, \quad 0 \le n \le N-1. \tag{11}$$

After taking the FFT of r_n^m, the frequency domain received signal on the k^{th} subcarrier of the m^{th} symbol is

$$y_k^m = \sum_{q=0}^{N-1} X_q^m h_q p_{k-q}^m + W_k^m, \quad 0 \le k \le N-1 \tag{12}$$

where X_q^m is q^{th} element of symbol vector X^m , h_q is the q^{th} element of channel vector, $\mathrm{h} = [h_0, h_1, h_2, \ldots, h_{N-1}]^T$, W_k^m is the AWGN in frequency domain and p_{k-q}^m is the $(k-q)^{th}$ spectral component of PHN spectral component vector, P^m , with modulo N indexing. Further, please note that with modulo N indexing, the lower order spectral components of PHN are given by p_0 , p_1, p_{N-1}, p_2, p_{N-2} , etc. For the convenience of the later analysis, it is preferable to represent the signal model in matrix form as

$$\mathbf{Y}^m = \mathbf{D}^m\mathbf{P}^m + \mathbf{W}^m \tag{13}$$

where $\mathbf{Y}^m = [y_0^m, y_1^m, \ldots, y_{N-1}^m]^T$,

$\mathbf{P}^m = \left[p_0^m, p_1^m, \ldots, p_{N-1}^m\right]^T$,

and $\mathbf{W}^m = [W_0^m, W_1^m, \ldots, W_{N-1}^m]^T$. $\mathbf{W}^m$ is an uncorrelated white noise vector distributed as $\Pr(\mathbf{W}^m) = \mathcal{CN}(0, 2\sigma_\omega^2\mathbf{I})$, with mean zero and covariance matrix $2\sigma_\omega^2\mathbf{I}$, which says:

$$\Pr(\mathbf{W}^m) = \frac{1}{(2\pi)^N \sigma_\omega^{2N}} \exp\left(\frac{-1}{2\sigma_\omega^2}\mathbf{W}^{mH}\mathbf{W}^m\right). \tag{14}$$

$\mathbf{D}^m$ is a column wise circulant matrix whose first column is vector $[h_0X_0^m, h_1X_1^m, \ldots, h_{N-1}X_{N-1}^m]^T$ and $\mathbf{h} = [h_0, h_1, h_2, \ldots, h_{N-1}]^T$,

$\mathbf{X}^m = \left[X_0^m, X_1^m, \ldots, X_{N-1}^m\right]^T$.

4. Joint MAP estimator/detector

In this section, we form a MAP estimate of the channel vector/symbol vector and the PHN spectral components ($\mathbf{P}^m$) jointly, given that $\mathbf{Y}^m$ is observed. For channel estimation stage, $\mathbf{X}^m$ is known and channel vector ($\mathbf{h}$) is estimated whereas in data detection phase $\mathbf{h}$ is known and symbol vector ($\mathbf{X}^m$) is estimated. Further, in derivation, the estimated vector is presented with $\mathscr{H}^m$ (Channel/Symbol vector). As a posterior distribution, $\Pr(\mathscr{H}^m, \mathbf{P}^m|\mathbf{Y}^m)$ is proportional to the "complete likelihood function", $\Pr(\mathbf{Y}^m, \mathscr{H}^m, \mathbf{P}^m)$, so by using Bayes' rule we can write

$$\Pr(\mathbf{Y}^m, \mathscr{H}^m, \mathbf{P}^m) = \Pr(\mathbf{Y}^m|\mathscr{H}^m, \mathbf{P}^m)\Pr(\mathscr{H}^m)\Pr(\mathbf{P}^m). \tag{15}$$

With no prior knowledge of $\mathscr{H}^m$, $\Pr(\mathscr{H}^m)$ is constant, and with PHN

model presented in section 2, the prior distribution of $\mathbf{P}^m$ is: $\Pr(\mathbf{P}^m) = \mathcal{CN}(0, \boldsymbol{\Theta})$, which says

$$\Pr(\mathbf{P}^m) = \frac{1}{\pi^N |\boldsymbol{\Theta}|} \exp\left(-\mathbf{P}^{mH} \boldsymbol{\Theta}^{-1} \mathbf{P}^m \right) \tag{16}$$

where $\boldsymbol{\Theta}$ is known. As it is equivalent to minimize the "complete negative log-likelihood function" and maximise the "complete likelihood function" in equation (15), so

$$\widehat{\mathscr{H}}^m, \widehat{\mathbf{P}}^m = \underset{\mathscr{H}^m, \mathbf{P}^m}{arg\ min} \{ -\log[\Pr(\mathbf{Y}^m | \mathscr{H}^m, \mathbf{P}^m)] - \log[\Pr(\mathbf{P}^m)] \}. \tag{17}$$

Given the signal model in equation (13) and the AWGN density in equation (14), the conditional density can be written as

$$\Pr(\mathbf{Y}^m | \mathscr{H}^m, \mathbf{P}^m) = \frac{1}{(2\pi)^N \sigma_\omega^{2N}} exp\left\{ \frac{-1}{2\sigma_\omega^2} (\mathbf{Y}^m - \mathbf{D}^m \mathbf{P}^m)^H (\mathbf{Y}^m - \mathbf{D}^m \mathbf{P}^m) \right\}. \tag{18}$$

Using equations (16)–(18), the joint MAP estimate can be given as

$$\widehat{\mathscr{H}}^m, \widehat{\mathbf{P}}^m = \underset{\mathscr{H}^m, \mathbf{P}^m}{arg\ min} \{ \mathscr{L}(\mathscr{H}^m, \mathbf{P}^m) \} \tag{19}$$

where

$$\mathscr{L}(\mathscr{H}^m, \mathbf{P}^m) = \frac{1}{2\sigma_\omega^2} (\mathbf{Y}^m - \mathbf{D}^m \mathbf{P}^m)^H (\mathbf{Y}^m - \mathbf{D}^m \mathbf{P}^m) + \mathbf{P}^{mH} \boldsymbol{\Theta}^{-1} \mathbf{P}^m \tag{20}$$

defines the joint MAP cost function, which is to be minimized simultaneously, for statistically optimal solution of $\widehat{\mathscr{H}}^m$ and $\widehat{\mathbf{P}}^m$ with respect to $\mathscr{H}^m$ and $\mathbf{P}^m$.

5. Cyclic gradient descent optimization

The problem of cost function minimization is challenging and is solved in this section with proposed cyclic gradient descent optimization algorithm. As equation (20) is not easily differentiable for $\mathscr{H}^m$, but with a fixed $\mathbf{P}^m$, by searching over a finite set of feasible symbol vector, we can minimize equation (20) with respect to $\mathscr{H}^m$. Further, as $\boldsymbol{\Theta}$ is a non-singular covariance matrix, $\boldsymbol{\Theta}^{-1}$ is possible and is positive semi definite matrix, which makes equation (20) a quadratic function in $\mathbf{P}^m$. Now for a possible solution of equation (19) with respect to $\mathbf{P}^m$, equation (20) should be holomorphic, means analytic in complex vector $\mathbf{P}^m$. Thus if $\mathscr{H}^m$ is fixed, cost function in equation (20) can be minimized by taking its conjugate gradient with respect to $\mathbf{P}^m$ and equate it to zero. We begin the optimization with some initial estimate of PHN spectral components, $\widehat{\mathbf{P}}^{m0}$. This estimate can be obtained by Least Square (LS) estimation of [3] or Minimum Mean Square Error (MMSE) estimation of [2]. At i^{th} iteration, the estimate of symbol vector can be calculated as

$$\widehat{\mathscr{H}}^{mi} = \underset{\mathbf{X}^m}{arg\min} \left\{ \left(\mathbf{Y}^m - \mathbf{D}^m \widehat{\mathbf{P}}^{mi} \right)^H \left(\mathbf{Y}^m - \mathbf{D}^m \widehat{\mathbf{P}}^{mi} \right) \right\}. \tag{21}$$

To find the minimiser of equation (21), an exhaustive grid search over a range of possible values of $\mathscr{H}^m$ can be used. However, it is essential to begin with the best estimate of $\mathbf{P}^m$ possible to avoid local minima. In particular, the random search method has proved more effective in high dimensional spaces [16] than potentially expensive exhaustive grid search method, which suffers from the "curse of dimensionality." To update the PHN spectral components estimate, we compute the conjugate gradient of the MAP cost function with respect to the vector $\mathbf{P}^m$. This gradient is given by:

$$\nabla_{\mathbf{P}^{m*}} \mathscr{L}(\mathscr{H}^m, \mathbf{P}^m) = \frac{1}{\sigma_\omega^2} (\mathbf{D}^{mH} \mathbf{D}^m \mathbf{P}^m - \mathbf{D}^{mH} \mathbf{Y}^m) + 2\boldsymbol{\Theta}^{-1} \mathbf{P}^m \tag{22}$$

where

$$\nabla_{\mathbf{P}^{m*}} \mathscr{L}(\mathscr{H}^m, \mathbf{P}^m) = \begin{bmatrix} \frac{\partial \mathscr{L}(\mathscr{H}^m, \mathbf{P}^m)}{\partial p_0^{m*}} \\ \frac{\partial \mathscr{L}(\mathscr{H}^m, \mathbf{P}^m)}{\partial p_1^{m*}} \\ . \\ . \\ \frac{\partial \mathscr{L}(\mathscr{H}^m, \mathbf{P}^m)}{\partial p_{N-1}^{m*}} \end{bmatrix}. \tag{23}$$

At iteration i, we fix the symbol vector in equation (22) so that $\mathscr{H}^m = \widehat{\mathscr{H}}^{mi}$. Then, by setting $\nabla_{\mathbf{P}^{m*}} \mathscr{L}(\mathscr{H}^m, \mathbf{P}^m)|_{\mathscr{H}^m = \widehat{\mathscr{H}}^{mi}}$ equal to zero and solving for $\mathbf{P}^m$, we obtain the next PHN spectral components estimate:

$$\widehat{\mathbf{P}}^{mi+1} = \left[\widehat{\mathbf{D}}^{mi^H} \widehat{\mathbf{D}}^{mi} + 2\sigma_\omega^2 \boldsymbol{\Theta}^{-1} \right]^{-1} \widehat{\mathbf{D}}^{mi^H} \mathbf{Y}^m. \tag{24}$$

This updating procedure for the symbol vector and PHN spectral components continues for $i = 0, 1, 2, 3\ldots$ till $\mathscr{L}(\widehat{\mathscr{H}}^m, \widehat{\mathbf{P}}^m)$ gets stabilized with $\widehat{\mathscr{H}}^{mi+1} - \widehat{\mathscr{H}}^{mi} / \widehat{\mathscr{H}}^{mi} < \varepsilon$ (preset threshold), or a number of iterations are reached.

6. Computational complexity

The computational complexity is a critical issue for an OFDM receiver design and is addressed by the aid of the FFT implementation with the complexity order of $\mathscr{O}(NlogN)$. The frequency domain analysis maintains its original motivation of easy single tap equalization and linear receiver design. In the case of PHN estimation, the frequency domain approach is always preferred over time domain as it allows the estimation of only a few lower-order PHN spectral components to mitigate nearly 100% of interference.

The computational complexity for the proposed joint MAP algorithm rest over evaluating equations (21) and (24). In equation (21), $\mathbf{Y}^m$ and $\widehat{\mathbf{P}}^m$ are vectors while $\mathbf{D}^m$ is a circulant matrix. Thus, each matrix-vector computation has complexity order of $\mathscr{O}(N)$. The applied random search method is computationally compact with a majority of addition and subtraction with few multiplications and no divisions [16]. The PHN estimation step of equation (24) is more critical as it involves inversion of a matrix with the complexity order of $\mathscr{O}(N^3)$. However, in the frequency domain analysis of proposed joint MAP algorithm, all the matrices in equation (24) are reduced in the size of $2Q+1 \times 2Q+1$, resulting the complexity order of $\mathscr{O}(i(2Q+1)^3)$, where $Q \ll N$.

7. Simulation results

Performance of the proposed joint MAP algorithm is simulated in this section for various system parameters, where each simulation point is conducted using 10,000 OFDM symbols in MATLAB. Simulation model is based on IEEE 802.11g like a system with 20 MHz of transmission bandwidth and 64 subcarriers. In data detection phase, 56 subcarriers are used as active subcarriers out of which 10 are pilot subcarriers. OFDM symbols are generated using 16-QAM and 64-point IFFT, and then prepended by the CP of length 16 samples before transmitting over the channel. The channel is AWGN or multipath channel as applicable. For multipath channel, the discrete sampled CIR is modelled as $L = 10$ tapped delay lines having an exponentially decreasing Power Delay Profile (PDP):

$$\alpha_l^2 = E\{|g(l)|^2\} = \frac{1}{\gamma} \exp(-0.5l), l = 0, 1, .., L-1 \tag{25}$$

where $\gamma = \sum_{l} \exp(-0.5l)$ is chosen to normalise the PDP to unit energy. The 64-point FFT of the received signal is taken after receiver PHN modelling followed by CP removal. The receiver PHN is modelled as Wiener process and celebrated O–U process for FR VCO and PLL VCO respectively as shown in Fig. 3. The PHN effect is estimated and then jointly optimized with channel estimation/data detection by using proposed joint MAP algorithm.For the channel estimation stage, the $\widehat{\mathbf{P}}^{m0}$ is obtained with LS estimation [3] with CPE correction [17]. For that channel has been LS estimated [18], without PHN. The initial estimate of $\mathbf{P}^{m}$ for data detection phase is obtained by LS estimation [3] using the order of approximation (Q) that equals to 4. The random search algorithm [16] is applied to find the minimiser of equation (21).

In Fig. 4, the MSE of the proposed channel estimation in the presence of PLL VCO for estimating normalised CTF against system Signal to Noise Ratio (SNR) for $i = 6$ and $Q = 4$, is compared with the posterior CRLB for an OFDM channel estimator without PHN distortion. MSE performance curves for the channel estimation with CPE correction only and non-iterative ML joint estimation of [4] are also simulated and presented in Fig. 4.

For channel estimation stage, the posterior CRLB for estimating the CTF, ($CRLB_{\mathrm{h}}$) is calculated as [19]:

$$CRLB_{\mathrm{h}} = L/SNR \tag{26}$$

and the MSE is obtained as:

$$MSE = \frac{1}{MN} \sum_{m=1}^{M} \sum_{n=0}^{N-1} \left(h_n^m - \widehat{h}_n^m \right)^2 \tag{27}$$

where M represents the number of simulated OFDM symbols.

In Fig. 4 the proposed joint MAP algorithm outperforms the conventional channel estimator with CPE correction only for a wide range of SNR. As shown in Fig. 4, to achieve the MSE $= 10^{-2}$, the proposed joint MAP algorithm shows 4 dB improvement in SNR over conventional method. This performance gap increases with the increase of the SNR, because random Inter-Carrier Interference (ICI) with high PHN levels has an advantage over CPE for large values of SNR [1]. As shown in Fig. 4, the proposed joint MAP algorithm achieves MSE $= 10^{-4}$ at SNR $= 33$ dB whereas the conventional method causes a significant SNR degradation in the estimation and produces an error floor.

It can also be observed from Fig. 4 that the proposed joint MAP algorithm shows better improvements than the non-iterative ML joint estimator [4]. As shown in Fig. 4, to achieve the MSE $= 10^{-2}$, proposed joint MAP algorithm shows 1 dB improvement in SNR over ML joint estimator [4]. It is because the proposed algorithm performs optimization before each iteration to combat the server sensitivity towards high PHN level. As we apply the statistical knowledge of the PLL PHN spectral components without the assumption of small PHN, this adds in the performance improvement even for the large SNR values. It can be observed from Fig. 4 that the proposed joint MAP algorithm achieves MSE $= 10^{-4}$ at SNR $= 33$ dB whereas the ML joint estimator [4] needs SNR $= 37$ dB which shows the improvement of 4 dB for higher SNR values.

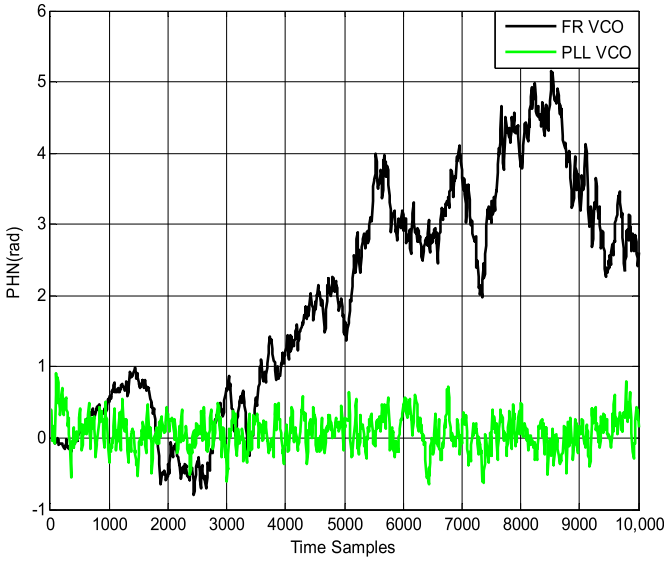

Fig. 3. Simulated PHN samples for FR VCO (Wiener process) and PLL VCO (Ornstein-Uhlenbeck process).

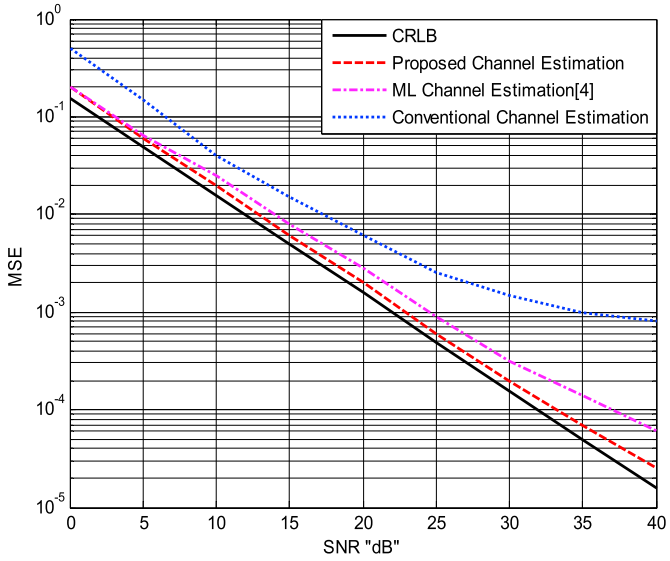

Fig. 4. Mse performance of CTF estimation as a function of SNR for PLL VCO PHN.

We now simulate the performance of the proposed joint MAP algorithm for data detection phase in the presence of applicable receiver PHN model and channel type. To illustrate the estimation accuracy and convergence behaviour of the algorithm, the generated PHN samples for FR VCO over one OFDM symbol are compared with estimated PHN samples in multipath channel for the different no. of iterations (i) with SNR $= 30$ dB and $Q = 4$. Fig. 5 shows that estimation approaches to the actual PHN when $i = 5$, and when with $i = 6$, it is very accurate.

In Fig. 6, the SER performance of the proposed joint MAP algorithm is compared with the "No PHN" scenario and conventional method of [2], for $i = 6$ and $Q = 4$, against system SNR in AWGN channel in the case of PLL VCO. The corresponding SER performance of the constrained MAP algorithm [8] is also simulated and presented in Fig. 6.

It can be observed from Fig. 6 that the proposed joint MAP algorithm achieves near "No PHN" performance whereas the conventional method [2] shows an error floor at higher SNR values. This happens because the inaccurate detection of symbols led to less accurate PHN spectral components estimation, and this error propagation at higher SNR values deteriorates the SER performance, which is compensated in the proposed algorithm with joint MAP optimization before the next iteration. It can also be observed from Fig. 6 that the constrained MAP algorithm of [8] underperforms in comparison with the proposed joint MAP algorithm even with the higher computational complexity. This happens because of the error produced during quantization operation and offline pruning. This performance gap increases with SNR because with high PHN dynamics, the error produced by PHN modelling mismatch dominates for high SNR.

In Fig. 7, the SER performance of the proposed joint MAP algorithm in the case of FR VCO is compared with the case of PLL VCO, for $i = 6$ and $Q = 4$, against concerned PHN bandwidth, $\Delta_{\mathrm{PN}} = \frac{\mathrm{PHN\ \ 3dBBW}}{\Delta \mathrm{f(subcarrier\ \ spacing)}}$, with system SNR $= 30$ dB, in multipath channel. The PLL VCO limits the single

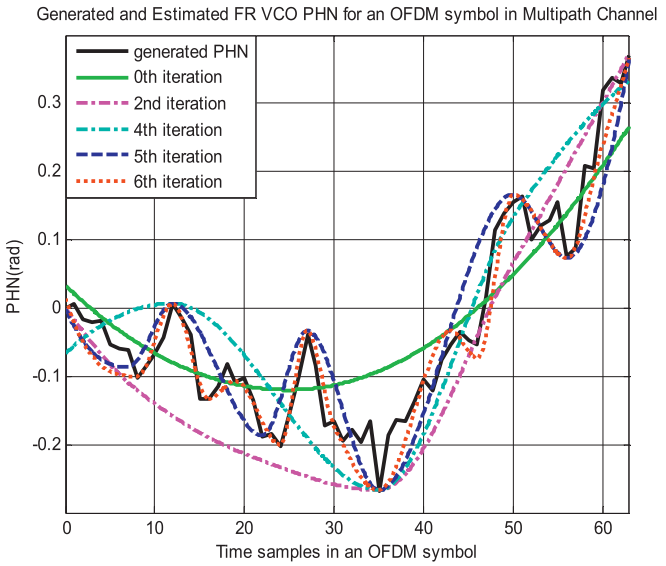

Fig. 5. FR VCO PHN estimation with proposed joint MAP algorithm for multipath channel.

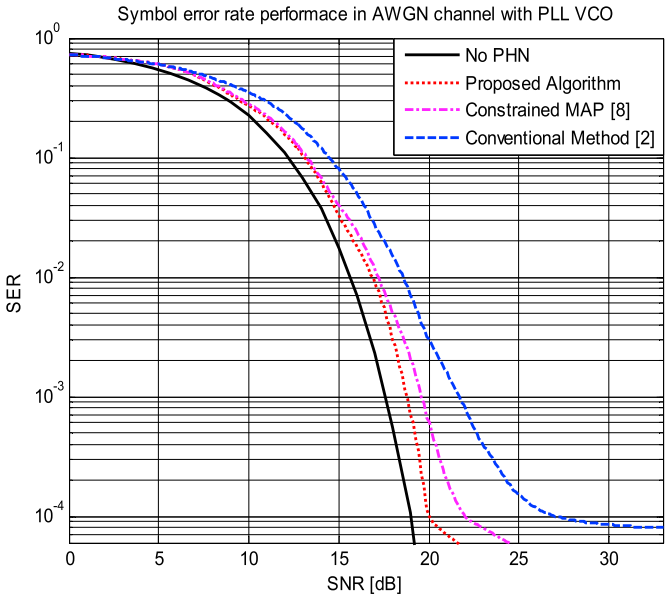

Fig. 6. SER performance comparison for AWGN channel in the case of PLL VCO.

direction drift of PHN process, and it reduces the overall PHN floor and then the CPE significantly. Simultaneously, the high frequency components of PHN are also suppressed with PLL VCO. With this double advantage of PLL VCO, the SER of the proposed algorithm shows the noticeable increment at very large Δ_{PN}, whereas it rises early at very small Δ_{PN} for FR VCO.

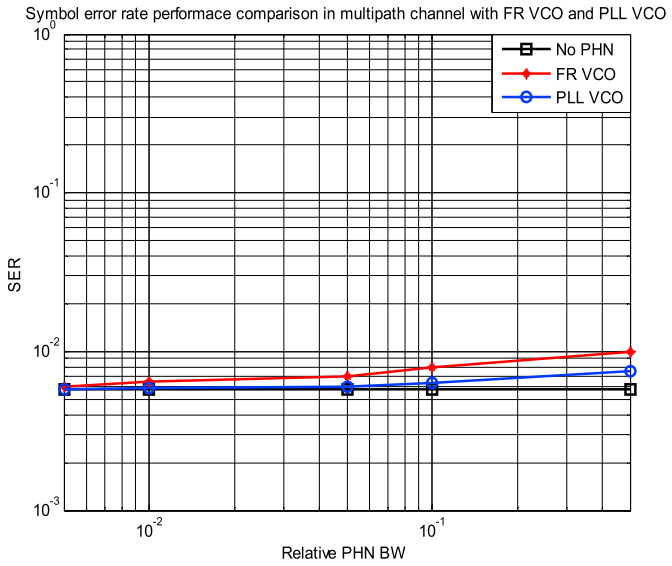

Fig. 7. SER performance comparison between the FR VCO and PLL VCO for proposed algorithm in multipath channel.

8. Conclusions

A new alternative of near-optimum channel estimation and data detection for the OFDM system in the presence of PHN, using joint MAP criterion, is presented in this paper. Two different models for time-varying PHN, produced by FR VCO and PLL VCO, are presented. Estimated PHN spectral component analysis improves over the cost function minimization and joint MAP estimation/detection. The simulation results show that with the proposed iterative cyclic gradient descent optimization algorithm, MSE approaches to CRLB and SER achieve near "No PHN" performance in the case of PHN modelling. Though the performance of the estimator improves with the order of approximation and number of iteration, incorporating the fading statistical study and soft extrinsic information will significantly improve the performance.

Declaration of competing interest

The authors whose names are listed immediately below certify that they have NO affiliations with or involvement in any organization or entity with any financial interest (such as honoraria; educational grants; participation in speakers' bureaus; membership, employment, consultancies, stock ownership, or other equity interest; and expert testimony or patent-licensing arrangements), or non-financial interest (such as personal or professional relationships, affiliations, knowledge or beliefs) in the subject matter or materials discussed in this manuscript.

Acknowledgments

Acknowledgment is made to the Department of Electronics and Communication Engineering, MNIT, for the support, and to anonymous reviewers and the Editor for their valuable suggestions and comments that helped to improve the presentation of the paper.

Appendix A

Ref.[12] has given equation (4) for the PLL VCO with loop filter of order one (Fig. 8) where:

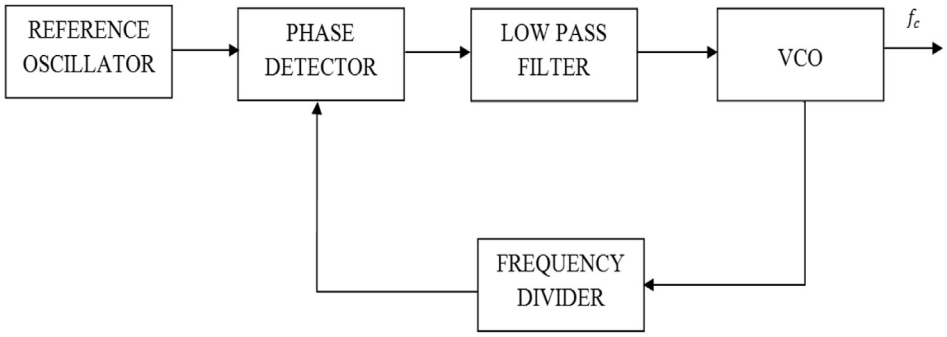

Fig. 8. Principal PLL Block Diagram.

$$\lambda_{1,2} = \frac{\omega_{lpf} \pm \sqrt{(\omega_{lpf}{}^2 - 4\omega_{lpf}\sqrt{C_{PLL}})}}{2},$$

$$\xi_1 = \frac{C_{in}\lambda_2}{(\lambda_1 - \lambda_2)\lambda_1},\ \xi_2 = \frac{-C_{in}\lambda_1}{(\lambda_1 - \lambda_2)\lambda_2},$$

$$\zeta_1 = \frac{C_{in} + C_{VCO}}{(\lambda_1 - \lambda_2)^2}\left(\frac{\lambda_2{}^2}{2\lambda_1} - \frac{\lambda_1\lambda_2}{2(\lambda_1 + \lambda_2)}\right),$$

and

$$\zeta_2 = \frac{C_{in} + C_{VCO}}{(\lambda_1 - \lambda_2)^2}\left(\frac{\lambda_1{}^2}{2\lambda_2} - \frac{\lambda_1\lambda_2}{2(\lambda_1 + \lambda_2)}\right)$$

where f_c is the centre frequency of VCO in Hz, ω_{lpf} is the angular corner frequency of the low pass filter in rad/sec, and $\sqrt{C_{PLL}}$ is the PLL bandwidth in Hz. C_{in} and C_{VCO} are diffusion rates of the reference oscillator and VCO, respectively.

References

[1] S. Wu, Y. Bar-Ness, OFDM systems in the presence of phase noise: consequences and solutions, IEEE Trans. Commun. 52 (11) (2004) 1988–1997.

[2] D. Petrovic, W. Rave, G. Fettweis, Effect of phase noise on OFDM systems with and without PLL: characterization and compensation, IEEE Trans. Commun. 55 (8) (2007) 1607–1616.

[3] V. Syrjälä, M. Valkama, N. Tchamov, et al., Phase noise modelling and mitigation techniques in OFDM communications systems, Proc. Wireless Telecommunications Symposium 1–7 (2009).

[4] P. Rabiei, W. Namgoong, N. Al-Dhahir, A non-iterative technique for phase noise ICI mitigation in packet-based OFDM systems, IEEE Trans. Signal Process. 58 (11) (2010) 5945–5950.

[5] O.H. Salim, A.A. Nasir, H. Mehrpouyan, et al., Channel, phase noise, and frequency offset in OFDM systems: joint estimation, data detection, and hybrid Cramer-Rao lower bound, IEEE Trans. Commun. 62 (9) (2014) 3311–3325.

[6] V.N.D. Nhat, T.B.T. Minh, C.T. Tan, et al., Joint phase noise and doubly selective channel estimation in full-duplex MIMO-OFDM systems, in: Proc. of the International Conference on Advanced Technologies for Communications, ATC, 2016, pp. 412–417.

[7] T.J. Lee, Y.C. Ko, Channel Estimation and Data Detection in the Presence of Phase Noise in MIMO-OFDM Systems with Independent Oscillators, IEEE Access, 2017.

[8] A. Ishaque, A. Gerd, Efficient MAP-based estimation and compensation of phase noise in MIMO-OFDM receivers, AEU-International Journal of Electronics and Communications 67 (12) (2013) 1096–1106.

[9] K. Lee, S.C. Lim, K. Yang, Blind compensation for phase noise in OFDM systems over constant modulus modulation, IEEE Trans. Commun. 60 (2012) 3.

[10] S. Negusse, P. Zetterberg, P. Händel, Phase-noise mitigation in OFDM by best MatchTrajectories, IEEE Trans. Commun. 63 (5) (2015) 1712–1725.

[11] A.O. Isikman, H. Mehrpouyan, A.A. Nasir, et al., Joint phase noise estimation and data detection in coded Multi-Input–Multi-Output systems, IET Commun. 8 (2014) 7.

[12] A.P. Ghosh, W. Qin, A. Roitershtein, Discrete-time Ornstein-Uhlenbeck process in a stationary dynamic environment, J. Interdiscipl. Math. 19 (1) (2016) 1–35, 2016.

[13] A. Demir, A. Mehrotra, J. Roychowdhury, Phase noise in oscillators: a unifying theory and numerical methods for characterization, IEEE Transactions on Circuits and Systems I: Fundamental Theory and Applications 47 (5) (2000) 655–674.

[14] A. Mehrotra, Noise analysis of phase-locked loops, IEEE Transactions on Circuits and Systems-I: Fundamental Theory and Applications 49 (9) (2002) 1309.

[15] D. Petrovic, W. Rave, G. Fettweis, Intercarrier interference due to phase noise in OFDM - estimation and suppression, in: Proc. IEEE Vehicular Technology Conference Fall, 2004, pp. 2191–2195.

[16] J.A. Nelder, R. Mead, A simplex method for function minimization, Comput. J. 7 (1965) 308–313.

[17] S. Wu, Y. Bar-Ness, A phase noise suppression algorithm for OFDM based WLANs, IEEE Commun. Lett. 6 (2002) 12.

[18] S. Coleri, M. Ergen, A. Puri, et al., Channel estimation techniques based on pilot arrangement in OFDM systems, IEEE Trans. Broadcast. 48 (2002) 3.

[19] K. Shrivastav, R.P. Yadav, K.C. Jain, Cyclic gradient descent optimization for joint MAP estimation of channel and phase noise in OFDM, IET Commun. (2017), https://doi.org/10.1049/iet-com.2017.0732.